Schöpa, A., Floess, D., Saint Blanquat, M., Annen, C., Launeau, P. (2015): The relation between magnetite and silicate fabric in granitoids of the Adamello Batholith. - *Tectonophysics*, *642*, p. 1-15.

DOI: http://doi.org/10.1016/j.tecto.2014.11.022

The relation between magnetite and silicate fabric in granitoids of the Adamello Batholith

A. Schöpa[a,*], D. Floess[b,c], M. de Saint Blanquat[d], C. Annen[a], P. Launeau[e]

[a] University of Bristol, School of Earth Sciences, Wills Memorial Building, BS81RJ Bristol, United Kingdom

[b] University of Geneva, Department of Earth Sciences, 13, Rue des Maraîchers, 1205 Geneva, Switzerland

[c] Université Lausanne, Batiment Geopolis, 1015 Lausanne, Switzerland

[d] GET, Obervatoire de Midi-Pyrénées, Université de Toulouse, CNRS, IRD, 14 avenue Edouard Belin, F-31400 Toulouse, France

[e] Laboratoire de Planétologie et Géodynamique de Nantes, CNRS/Université de Nantes, F-44322 Nantes, France

* Corresponding author at: Helmholtz Centre Potsdam, GFZ German Research Centre for Geosciences, Telegrafenberg, D-14473 Potsdam, Germany.

E-mail address: schoepa@gfz-potsdam.de (A. Schöpa).

Tectonophysics 642 (2015) 1–15

http://dx.doi.org/10.1016/j.tecto.2014.11.022

Article history:

Received 3 February 2014; Received in revised form 13 October 2014; Accepted 23 November 2014; Available online 18 December 2014

Keywords:

Rock fabrics in granites; X-ray micro-tomography; Anisotropy of magnetic susceptibility (AMS); 3D shape fabrics (SPO); Magnetic interactions

Abstract

The link between the macroscopic silicate fabric and the magnetite-controlled AMS (anisotropy of magnetic susceptibility) fabric in ferromagnetic rocks was investigated through a comprehensive comparison between different fabric measurement techniques. Sample lithologies include tonalites and granodiorites from the Lago della Vacca Complex, Adamello Batholith, Italy. The datasets used to assess the link between subfabrics and the coherence between methods include: 1) macroscopic silicate fabric measured directly in the field; 2) macroscopic silicate fabric derived from image analysis (IA) of outcrop pictures and sample pictures; 3) shape-preferred orientations (SPO) of mafic silicates, 4) SPO of magnetite, and 5) calculated distribution of magnetite grains from computer-assisted high-resolution X-ray tomography (X-ray CT) images; 6) fabrics derived from the AMS. Macroscopic mineral fabrics measured in the field agree with the IA results and with the SPO of mafic silicates obtained from the X-ray CT imaging. The X-ray CT results show that the SPO of the magnetite grains are consistent with the AMS data whereas the spatial distribution of the magnetite grains is less compatible with the AMS fabric. This implies that the AMS signal is mainly controlled by the shape of the magnetic carrier mineral rather than by the spatial arrangement of the magnetite grains. An exception is the presence of magnetite clusters. Furthermore, the SPO of mafic silicates and the SPO of the magnetite grains are consistent with the AMS data. Another finding of this study is that the magnetic susceptibility correlates linearly with the amount of magnetite in the samples. The coherent results obtained from a variety of methods reinforce the application of both AMS measurements and IA as robust tools to analyse fabrics in granitic intrusions.

1. Introduction

Anisotropy of magnetic susceptibility (AMS) has been widely applied to analyse fabrics in magmatic intrusions (e.g. Archanjo et al., 2012; Bouchez, 1997; Cruden et al., 1999; Gleizes et al., 1998; Launeau and Cruden, 1998; López de Luchi et al., 2004; Petronis et al., 2012; Raposo et al., 2012; St Blanquat et al., 2001), lava flows (e.g. Cañón- Tapia and Coe, 2002; Cañón-Tapia, 2004; Loock et al., 2008), and dykes (e.g. Archanjo and Launeau, 2004; Cañón-Tapia and Chávez- Álvarez, 2004; Eriksson et al., 2011; Geoffroy et al., 2002). Many studies showed that the magnetic fabric obtained by AMS measurements is commonly coaxial with the macroscopic silicate fabric in ferro- and paramagnetic rocks (e.g. Aranguren et al., 2003; Archanjo et al., 1994; Hrouda et al., 1999; Petronis et al., 2004) and hence can be used to gain information about magma flow, emplacement related strain and/ or tectonic strain. However, the AMS signal cannot be compared directly to the shape-preferred orientation (SPO) of the main silicate minerals that determine the macroscopic fabric of the rock. The relation between AMS fabric and strain is not simple either (Hrouda and Ježek, 1999): Arbaret et al. (2013) showed that AMS and SPO fabrics in simple shear flow tend to stabilise parallel to the shear plane only at high strain and that the amount of strain required for fabric stabilisation depends on the aspect ratio of the particles and their initial orientation. Adding further complexity, the magnetic axes and the three-dimensional shape of the magnetic minerals are not always clearly associated (Bouchez, 1997).

Theoretical and experimental work has been conducted to explore the nature of the AMS signal in ferromagnetic igneous rocks where magnetite is the main magnetic carrier mineral of the AMS. Two theories explaining how the AMS signal is controlled were developed:

i) The AMS signal is attributed to the shape anisotropy of the magnetite grains (O'Reilly, 1984). Although magnetite crystallises in the cubic system the grains are not necessarily isometric. It was demonstrated that the AMS ellipsoid and the shape ellipsoid of the magnetite grains (SPO) are closely related in terms of orientation and intensity of the ellipsoids' axes (Grégoire et al., 1998).

ii) The AMS signal is attributed to the irregular distribution of the magnetite grains and their tendency to form clusters (Hargraves et al., 1991; O'Reilly, 1984; Stephenson, 1994). The distribution anisotropy of the magnetites leads to varying magnetic interactions between the magnetite grains and create the AMS signal (Cañón-Tapia, 1996). Clusters of magnetite grains result in an increased or de creased magnetic susceptibility along the clusters' longest axes, de pending on whether the grains are aligned or side-by-side (Grégoire et al., 1995). Therefore, the grain shape of the magnetites and the magnetic anisotropy degree might not be closely related.

To synthesise these two concepts about the origin of the AMS signal, studies showed that the AMS signal is controlled by several factors, such as the proportion of grains that interact magnetically or not, the shape of these grains, and intrinsic material properties of the magnetic grains (Cañón-Tapia, 2001). Numerical models and experiments suggest that the two end-members of magnetic interactions between grains are i) small magnetite grains, which form clusters and interact magnetically, determine the AMS signal by their distribution, and ii) large, dispersed magnetite grains do not interact magnetically and control the AMS signal by their preferred shape orientation (Gaillot et al., 2006). Quantifying the contributions of each of these factors to the AMS signal remains a major challenge as the signal only gives integrated information over the whole volume of the sample.

A recent study uses high-resolution X-ray tomography (X-ray CT) as a non-destructive technique to shed light into the distribution and shape of magnetite grains in tonalites (Floess, 2013). The conclusion of this work is that the distribution of the magnetite grains only influences the AMS

signal if the magnetites are arranged in clusters, in agreement with Gaillot et al. (2006). If a strong AMS is present in the rock, the AMS ellipsoid is identical to the shape and the preferred orientation of the magnetite grains. However, the connection of AMS fabric to the SPO of the main silicate phases (i.e. macroscopic fabric) remains solely observational.

Like this non-quantified relation, the link between the magnitude of the mean magnetic susceptibility K_m and the amount of iron has not been investigated in detail for highly ferromagnetic rocks. It has only been proposed for rocks with K_m smaller than 10^{-3} SI that K_m correlates positively and linearly with the iron content of those rocks (Bouchez, 1997; Rochette, 1987).

Building upon the work of Floess (2013), this paper presents a detailed comparison between different fabric analysis measurements in ferromagnetic granitoids of the Lago della Vacca Complex (LVC), Adamello Batholith. The aims of this study are to test the applicability of the methods to characterise fabrics, to explore the link between AMS fabric and the macroscopic silicate fabric, to determine the origin of the AMS signal and to explore the relation between the magnetic susceptibility and the magnetite content. The purpose of this paper is not to discuss the fabric results in the context of the regional geology of the LVC, which is covered in another paper (Schöpa et al., submitted for publication).

2. Samples and methods

2.1. Samples

The 12 samples selected for this study were taken in the LVC, a silicic intrusion in the southern Adamello Batholith (Fig. 1). The samples are made up of Lago della Vacca tonalite, Galliner granodiorite and marginal tonalites. A full description of the microstructures of these rocks is given by John and Blundy (1993) and will be summarised here.

The Lago della Vacca tonalite shows an equigranular texture with 1–3 mm large prismatic hornblende, subhedral plagioclase, subhedral biotite, euhedral titanite and anhedral apatite (samples 11AS11, 11AS25, 11AS38, 11AS39, 11AS53). Quartz and alkalifeldspar smaller than 2 mm are present in the interstices. The hornblende and the titanite occasionally contain inclusions of plagioclase, pyroxene and oxides.

The equigranular Galliner granodiorite is characterised by prismatic hornblende crystals and subhedral plagioclases of 2–3 mm in size (samples 11AS47, 11AS58). Subhedral biotite with apatite, plagioclase and oxide inclusions is subordinately present. Interstitial quartz and alkalifeldspar are usually smaller than 3 mm.

Marginal tonalites of the LVC include two varieties: i) highly foliated tonalite, where up to 6 mm large plagioclase and lath-shaped horn blende crystals define the macroscopic foliation (samples 11AS12, 11AS28, 11AS40, 11AS52), and ii) tonalite with equigranular hornblende crystals up to 4 mm in size with inclusions of anhedral plagioclase, pyroxene and oxides (sample 11AS46). Interstitial plagioclase, biotite, quartz and alkalifeldspar measure 0.2–1 mm in both marginal tonalite varieties.

Oxides, predominately pure magnetite, are present in the tonalites and granodiorites of the LVC as individual grains or grain clusters. Single oxide grains occur in the groundmass, fill in the interstices between the silicate minerals and are included in larger hornblende, plagioclase, biotite and titanite crystals. The magnetite inclusions are occasionally located parallel to the rims of the

host crystal. If large hornblende crystals have a preferred orientation single magnetite crystals and mag netite clusters follow this alignment (Fig. 2). Individual magnetite grains measure between 30 and 500 μm, average ~ 150 μm, and magnetite clusters can be up to 550 μm large.

2.2. Field measurements and image analysis (IA)

The macroscopic silicate fabric in the LVC granitoids is determined by the preferred orientation of mafic silicates such as lath-shaped hornblendes and subordinate, anhedral biotites. Magmatic foliations were measured directly in the field with a geological compass; mineral lineations could not be resolved at outcrops.

IA with the intercept method in grey levels (Launeau et al., 2010) quickly analyses the whole crystal shape anisotropy of a rock by a smoothed detection of boundaries between contrasted mineral phases. The division of the area of analysis (or mineral area when available) by the number of boundaries counted in each direction gives the mean intercept length rose. This is the mean shape preferred orientation of the minerals (SPO) because it is proportional to the preferred orientation of the minerals' shape towards a main direction. Since most of the fabrics or SPO are ellipses in 2D, we can calculate the 3D SPO ellipsoid with a minimum of three mutually perpendicular images (Launeau and Robin, 2005; Robin, 2002). It includes an adjustment of the size in sections to make them compatible with a common ellipsoid. The method finally provides a preferred orientation of crystal population along a main direction, expressed as the longest axis of the SPO fabric ellipsoid.

The intercept method was applied to two image datasets to deter mine the macroscopic SPO of mafic silicate crystals marked by their contrast to quartz and feldspar. One image dataset was taken of rock surfaces in the field (IA-F) and the second dataset was obtained from rock samples (IA-S) cut in the laboratory (Fig. 3). These were the same samples that were cored for the AMS analysis and used for the X-ray CT measurements.

The intercept method in grey levels can rapidly quantify the macroscopic silicate fabric. However, the method can only be used if sufficient minerals of different brightnesses are present in the images. In addition, the SPO of the IA is sensitive to shape variations of the mafic silicates. In our sampled lithologies, the general habit of the hornblende and biotite crystals does not change significantly in individual samples or across each sample field site. Hence, our results of the IA can be used to quantify the strength of the fabric in individual samples/sites and can be compared to other fabric measurements performed at the same sample/site. Table 1 summarises the characteristics of the fabric measurement techniques with investigated minerals, area/volume analysed and resolution of the imaging techniques.

2.3. Anisotropy of magnetic susceptibility (AMS)

Oriented block samples were collected in the field, reoriented in the laboratory and cored for AMS measurements. 2.2 cm high right circular cylinder specimens with a diameter of 2.5 cm were cut from the cores. The AMS signal of six to nine cylinder specimens for each sample site was measured with an AGICO KLY-3 Kappabridge (Agico, Brno, Czech Republic) working at an applied field of 300 A/m and a frequency of 875 Hz at the Géosciences Environnement Toulouse laboratory, France. The AMS is represented by an ellipsoid with three major axes reflecting the maximum, intermediate and minimum directional strength of the magnetic susceptibility. For our samples, the AMS is homogeneous for all sample specimens of one sample site.

Optical microscopy on thin sections, SEM, thermomagnetic and hysteresis measurements revealed that large, multi-domain magnetite grains are the dominant magnetic phase in all samples of the LVC (Schöpa et al., submitted for publication). The AMS of multi-domain

magnetites is usually "normal" where the magnetic axes are directly related to the three-dimensional shape of the magnetite crystal and the longest axis of the grain is parallel to the largest susceptibility axis (Rochette et al., 1999). The samples have a high mean susceptibility K_m ranging from 18 to 119 × 10^{-3} SI (Table 2), consistent with micro- structural observations that the samples contain approximately 3% magnetite (cf. John and Blundy, 1993; John and Stünitz, 1997).

2.4. High-resolution X-ray tomography (X-ray CT)

One AMS core specimen per sample site was selected for the X-ray CT imaging. The X-ray CT analyses were performed at the Université de Lausanne, Switzerland, with a SkyScan 1173 high-energy spiral scan on 12 of the core samples that had been measured for the AMS. The X-ray source operated at 130 kV and 61 μA, and the X-rays were detected with a flat panel sensor of 2240 × 2240 pixel (Fig. 3). As the linear attenuation coefficient of X-rays passing through an object is related to the density, the atomic number and the X-ray beam energy, the grey scales in the detected shadow images represent minerals of different densities (Ketcham, 2005a). The attenuation coefficient of magnetite is much larger than that of quartz and other silicate minerals allowing for a good distinction between magnetite and silicate phases (Baker et al., 2012).

NRecon from SkyScan was used for reconstructing stacks of horizontal slice images from the acquired shadow images. Post-processing of the tomography scans, including post-alignment of the X-ray beam (Feldkamp et al., 1984), beam-hardening correction and ring-artefact correction were performed to obtain homogeneous grey-levels for each mineral phase in all the slice images of one sample. One pixel had the dimension of 23 μm throughout the post-processing and the fol lowing phase analysis. The software Blob3D was able to threshold and separate magnetite and the mafic silicates (hornblende and biotite), from the other phases, mainly quartz and feldspar in the reconstructed images (Ketcham, 2005b).

From the magnetite and the mafic silicate fraction, the bulk shape anisotropy for individual magnetite grains or magnetite clusters and for the mafic silicates are calculated as star length distribution (SLD) in Quant3D (Ketcham, 2005a). Similar to the intercept method of the IA, the star analyses explore the surrounding volume for the detection of boundaries. Unlike IA, which explores the whole image, the star pro cess starts from a subset of nodes and looks for the first boundary in any direction permitted by the network of voxels. Thus, it is not sensitive to noisy detection of boundaries along complex imbrications of cubes forming a mineral phase. For the SLD method, the grain shape anisotropy is visualised by an ellipsoid. The axes lengths of the fabric ellipsoids of the SLD can be directly compared to the axes lengths of the fabric ellipsoids obtained from different methods such as IA and AMS.

2.5. Distribution anisotropy

In the X-ray CT images, the volume and the midpoint coordinates of the magnetite grains were extracted by Blob3D and used to calculate the distribution anisotropy of the most voluminous magnetite grains with a Matlab programme (Floess, 2013). First, the orientation of the line be tween two grains is determined for all grain pairs. Then, these orientations are weighted by the volumes V_1 and V_2 of the two grains and the distance r between them with a weighing factor

$$w = \frac{V_1 + V_2}{\pi r^3} \qquad (1)$$

(Stephenson, 1994). We evaluated the effect of the number of (size- sorted) magnetite grains on the calculation of the distribution anisotropy. Calculations were run with the 500, 700, 1000, 1200 and 1500 most voluminous magnetite grains. We found that the distribution anisotropy is only

marginally affected by the number of grains used in the calculations and therefore, we only present the results of the calculations with the 1000 most voluminous grains.

3. Results

Each independent fabric measurement technique used in this study provides a fabric ellipsoid, which determines the orientation, shape and strength of the respective fabric. An exception is the mafic silicate fabric measured in the field, which only delivers foliations and no fabric ellipsoid. The longest axis of a fabric ellipsoid defines the lineation and the shortest axis is the pole to the foliation. Oblate fabric ellipsoids indicate that the fabric is dominated by planar structures (foliations) whereas prolate ellipsoids are characteristic for fabrics dominated by linear structures (lineations). The results of the fabric measurements are given in Table 2.

3.1. Relation between the SPO of silicates and magnetite

A detailed comparison between the field foliations, IA-F, IA-S and the AMS on the intrusion-scale in the LVC yield that the AMS is usually co- axial with the SPO of the mafic silicates defining the macroscopic fabric (Schöpa et al., submitted for publication). In addition to the orientations, the shapes of the IA-F and IA-S SPO ellipsoids and of the AMS ellipsoid for the 66 sample sites agree. For the subset of this study, angular departures between the foliations of the field, IA-F, IA-S and the AMS do not exceed 45° (Fig. 4). Small discrepancies are due to uncertainties in the field measurements, reorientation of the AMS samples and uncertainties in sample mounting in the AMS instrument.

The foliations obtained from the SLD ellipsoid of the mafic silicates plot no more than 48° from the foliations acquired in the field. The lineations and foliations of the SLD (black circles in Fig. 4) are also in agreement with the foliations and lineations obtained from IA-F, IA-S and AMS. This correlation is expected because the mafic silicates SLD represents the SPO of the hornblendes and biotites and should hence be consistent with the field measurements of the mafic silicate fabric and the IA-F and IA-S.

Likewise, the directional fabric components of the magnetite SLD (black squares in Fig. 4) have the same orientation as the field, the IA- F, IA-S, the SLD of the mafic silicates and the AMS. As one would expect, the AMS of the sample cores selected for the X-ray CT generally plot closer to the magnetite SLD than the averaged AMS for all cores of one site. Correspondingly, the averaged AMS is usually closer to the IA-F, IA-S and the field measurements than to the magnetite SLD.

3.2. Intensity of SPO

The shape of fabric ellipsoids delivered by different techniques can easily be compared in a plot of the axial ratios of the ellipsoids (Woodcock, 1977). In such a Flinn-type diagram (Flinn, 1962), the lines radiating out from the origin divide regions of different fabric ellipsoid shapes such as prolate ($\infty > K > 1$) where the maximum (max) axes cluster in a stereonet projection, and oblate shapes ($1 > K > 0$) where the maximum and the intermediate (int) axes form a girdle.

$$K = \frac{\ln (max/int)}{\ln (int/min)} \qquad (2)$$

is the gradient of the radiating lines (Woodcock, 1977).The Flinn-type diagrams of our samples show that the shape of the fabric ellipsoids are mainly in good agreement for the IA-F, IA-S, AMS, the mafic silicates SLD and the magnetite SLD (Fig. 5). Especially for samples 11AS11, 11AS28, 11AS40 and 11AS52, the axial ratios of the different techniques plot along one line,

representing one distinctive fabric shape. Oblate fabrics dominate for samples 11AS11, 11AS12, 11AS28, 11AS38, 11AS39, 11AS40, 11AS46, and 11AS52. Prolate fabrics prevail in samples 11AS53 and 11AS58. The other samples plot in the transitional area around K = 1. The oblate character of the fabric is also clearly visible for samples 11AS11, 11AS40 and 11AS46 in Fig. 4a, g and h where the foliation poles for the different fabric analysis techniques cluster and the lineations plot along a great circle.

The intensive parameters P% = 100(max/min – 1), F% = 100(max/int – 1), L% = 100(int/min – 1), and the shape parameter T = (2(ln int – ln min))/(ln max – ln min) – 1 (Jelinek, 1981) can also be calculated from the main axes of the fabric ellipsoids. A comparison of the fabric intensity as provided by these parameters confirms our finding that the strength of the AMS fabric is in good agreement with the intensity of the SPO of the magnetite (Table 3 and Fig. 6a and c).

3.3. Relation between silicate SPO and the 3D spatial distribution of magnetite

The orientations of the main axes of the distribution anisotropy ellipsoids, which are a measure of the spatial arrangement of the magnetite grains, are less consistent with the other fabric measurements. Very large angular departures to field, IA-F, IA-S, AMS and SLD data are no ticeable for many samples (Fig. 4: 11AS25, 11AS28, 11AS46, 11AS53 and 11AS58). For some samples, the foliation poles of the AMS plot in between the poles of the distribution anisotropy and the magnetite SLD, e.g. samples 11AS11, 11AS28, 11AS39 and 11AS47.

If magnetite grains are distributed in well-defined, widely-spaced planes (e.g. foliations) their distribution anisotropy should plot in the region where K b 1 in the Flinn-type diagrams (Floess, 2013). Similarly, if the magnetite grains are distributed in lines (e.g. lineations) their distribution anisotropy should plot in the region where K N 1. Randomly distributed magnetite grains should plot close to the origin. The axial ratios of the distribution anisotropy ellipsoids are mostly inconsistent with the other fabric datasets (Fig. 5). The distribution an isotropy plots close to the axial ratios of the AMS ellipsoid only for samples 11AS39, 11AS40 and 11AS46. The grain distribution is often less oblate (K b 1) than indicated by the SPO ellipsoids. For samples 11AS11, 11AS25, 11AS38, 11AS52 and 11AS53, the distribution anisotropy shows a trend towards smaller aspect ratios with increasing number of grains considered in the calculations (not shown in Fig. 5). As these additional grains have smaller volumes, this trend could indicate that the smaller magnetite grains are more randomly distributed than the larger grains. The intensity of the distribution anisotropy of the magnetite grains is not in good agreement with the strength of the AMS fabric (Fig. 6b and d).

3.4. Susceptibility and magnetite content

Since the volume of each separated magnetite grain in the tomographic samples was extracted by the software Blob3D, the total volume of magnetite in each core specimen could be calculated and related to the sample volume (Table 4). The magnetite content accounts for 0.2–1.4 vol% for samples with mean susceptibilities K_m of 18–119 × 10^{-3} SI and correlates positively with K_m of individual sample cores (Fig. 7a) following the linear relationship:

$$\text{vol\%-mgt} = 0.0126 \times K_m\,(10^{-3}\,\text{SI}) - 0.131. \quad (3)$$

For the integrated K_m of all sample cores of one field site, the linear fit is less excellent but still good with $R^2 = 0.91$, compared to $R^2 = 0.94$ for K_m of the individual core measurements. The number of magnetite grains separated in each sample core is also directly proportional to K_m with higher K_m for sample cores with a larger number of magnetite grains (Fig. 7b).

4. Discussion

4.1. Relation between the SPO of silicates and magnetite

Within ferromagnetic rocks (i.e., magnetite-bearing intrusives such as the Vacca pluton), the AMS signal results from the mean shape orientation (SPO) and the arrangement of all ferromagnetic minerals (Archanjo et al., 1995; Grégoire et al., 1995). The paramagnetic (Fe- Mg silicates) contribution is typically negligible because of the very high intrinsic magnetic susceptibility of magnetite. Consequently, in this type of magmatic rocks, AMS (magnetite subfabric) and IA (subfabric of silicates) are complementary, and their combination has proven to be highly useful to reconstruct the emplacement dynamics of intrusive magmas (e.g. Archanjo et al., 2002; Archanjo et al., 2009, 2012; Diot et al., 2003) and to infer flow characteristics of ignimbrites and basaltic lava flows (e.g. Boiron, 2011; Gountié Dedzo et al., 2011). These studies found that petrofabric and magnetic AMS fabric are generally spatially coincident, i.e. coaxial. Our results confirm this observation and add data about fabric intensity, grain shape, and distribution characteristics obtained from X-ray CT imaging.

Our results show that the magnetite and mafic silicate subfabrics are not only coaxial but also share the same range of values of intensity parameters. This confirms that IA can be used for quantitative fabric acquisition as a valid substitute for AMS. Moreover, the three methods (AMS, IA and X-ray CT imaging) appear as equivalent for the quantification of the fabric in this kind of ferromagnetic intrusive rocks.

The SLD of the mafic silicates and the SLD of the magnetites generally agree with the AMS and the field measurements, the IA-F and IA-S. Differences between the methods can partially be attributed to the technique of fabric acquisition and uncertainties in sample reorientation and mounting in the different instruments. The IA with the intercept method calculates a SPO fabric from the boundaries between crystals of different brightnesses along parallel scan lines across an image, without any a priori grey-scale thresholding. The SLD represents a bulk fabric based on the SPO identified from a tomographic image after applying a threshold to separate the phase(s) of interest (Ketcham, 2005a).

Fabric measurement techniques that cover a relatively large rock volume or surface area (field measurements, IA-F, IA-S, averaged AMS signal of all cylinder specimens from one sample site) usually plot close together in the stereographic projections. In turn, techniques that investigate one individual core specimen (AMS core, magnetite SLD and mafic silicates SLD) show a strong correlation. Consequently, small differences in the fabric between sample specimens from the same sample site exist but these differences are minor as the integrated methods for one sample site yield the same results.

4.2. Source of magnetic anisotropy: Grains vs. clusters

In our dataset, the orientation and shape of the magnetite SLD ellipsoids agrees well with the AMS ellipsoids, which indicates that the SPO of individual magnetite grains and of magnetite clusters deter mines the AMS signal. Although magnetite crystallises in the cubic crystallographic system, thin section analysis, SEM and X-ray CT imaging revealed that most grains have a shape anisotropy and are often organised in non-equidimensional grain clusters.

Besides the consistency between AMS fabric and mean grain shape of the magnetite grains and clusters, the arrangement of grains, i.e. the distribution anisotropy, is generally less consistent with the AMS and the magnetite SPO. The distribution anisotropy only shows the same directional fabric components as the AMS and the other fabric measurements in samples 11AS47 and 11AS52. The identical orientation of the grain distribution is due to magnetite clusters (cf.

Floess, 2013). The presence of magnetite clusters in our samples was confirmed by X-ray CT images, thin section and SEM analysis (Fig. 8). Difficulties to interpret the controls of the AMS signal also arise if the orientation of the AMS main axes plots between the axial orientations of the SLD and the distribution ellipsoid, e.g. samples 11AS39, 11AS47 and 11AS53. In those cases, where the magnetite SLD, the distribution anisotropy and the AMS ellipsoids show consistent orientations in the stereographic projections, the Flinn-type diagrams can be used to inspect whether or not the shape of the distribution ellipsoid and the shape of the other fabric ellipsoids differ from the AMS ellipsoid. For those samples with compatible orientations of the ellipsoids, the axial ratios of the distribution anisotropy diverge from the axial ratios of the AMS. In contrast, the AMS ellipsoid usually has the same shape as the SLD and the IA ellipsoids. Hence, the influence of the grain distribution on the AMS signal is small if the magnetites are not organised in clusters, in agreement with previous studies (Floess, 2013; Gaillot et al., 2006).

Our three-dimensional analysis of the magnetite content as derived from X-ray CT imaging combined with the AMS measurements enables to establish an empirical relationship between the amount of ferromagnetic minerals and K_m in granitoid samples. Although the general relation that K_m increases with higher magnetite content is know (Bouchez, 1997; Rochette, 1987), we are the first, to our knowledge, to relate K_m directly to the vol% of ferromagnetic minerals in ferromagnetic tonalites and granodiorites. However, the linear relationship be tween K_m and vol% of magnetite grains presented herein does not take the composition of the magnetite into account, which could deviate from the pure Fe_3O_4 composition when incorporating titanium (solid solution with ulvöspinel, Fe_2TiO_4). The constants of the linear equation relating K_m and magnetite content in Eq. (3), slope and the intercept with the y-axis, are a function of the magnetite composition and it is worthwhile investigating this dependence on magnetite composition in future studies. EDX analysis of our samples revealed that the magnetite grains are of nearly pure Fe_3O_4 composition with less than 1 wt.% titanium oxide confirming the first order link between K_m and magnetite content in ferromagnetic granitoids. This is supported by the thermo- magnetic curves which show a Curie temperature of about 575 °C, indicative for pure magnetite as the main magnetic carrier mineral of the AMS signal.

Our data also show a positive correlation of K_m with the number of magnetite grains in the samples, although the linear fit is of poorer quality than the K_m-magnetite amount relation. This higher variance could reflect the influence of grain clusters, which was confirmed with petro graphic observations.

5. Conclusions

Ferromagnetic, granitoid samples of the LVC in the Adamello Batholith were investigated with various fabric measurement techniques in order to constrain the relation between SPO of silicate and magnetite, to determine the relation between the 3D spatial distribution of magnetite grains and their SPO, and finally to determine the respective accuracy and efficiency of these methods.

In our samples, which all contain magnetite, the orientation and intensity parameters of the AMS signal are in remarkable agreement with the same parameters obtained with IA and X-ray CT. This indicates that those methods are able to give quantitative information about fabric strength, which is a new and original result, as previous studies use them only as qualitative tools (St Blanquat et al., 2001, 2006). In addition, we were able to show that the mean magnetic susceptibility K_m correlates linearly to the vol% of magnetite and to the number of magnetite grains in the analysed tonalites and granodiorites.

Our results demonstrate that the AMS signal is primarily controlled by the shape of magnetite

grains and magnetite clusters, and not by the distribution of the grains. The spatial arrangement of the magnetites is only relevant if the magnetite grains form clusters. In most of our samples, the SPO of magnetites and mafic silicates tends to be tabular (oblate ellipsoid) whereas the grain distribution anisotropy tends to be more linear (prolate ellipsoid). The AMS and the SPO of magnetites and of mafic silicates show similar fabrics in the analysed tonalites and granodiorites, which validates the application of AMS measurements and IA to investigate orientation and intensity of fabrics in granitoids.

List of Abbreviations

AMS Anisotropy of magnetic susceptibility

IA Image analysis

IA-F Image analysis field pictures

IA-S Image analysis sample pictures

LVC Lago della Vacca Complex

SEM Scanning electron microscope

SLD Star length distribution

SPO Shape-preferred orientation

X-ray CT Computer-assisted high-resolution X-ray tomography

Acknowledgements

This study was financed by ERC Advanced Grant "VOLDIES" (PI Steve Sparks) providing support to AS and CA. ERC Advanced Grant "CRITMAG" (PI Jon Blundy) provided funding for travel. We thank A. Winpenny, M. Hitchinson and L. Caricchi for their assistance in the field. L. Baumgartner is kindly acknowledged for providing the X-ray CT facilities. Discussions with Steve Sparks improved earlier versions of the manuscript. We also acknowledge the editor and two anonymous reviewers for their helpful comments.

References

Aranguren, A., Cuevas, J., Tubia, J., Roman-Berdiel, T., Casas-Sainz, A., Casas-Ponsati, A., 2003. Granite laccolith emplacement in the Iberian arc: AMS and gravity study of the La Tojiza pluton (NW Spain). J. Geol. Soc. Lond. 160 (3), 435–445.

Arbaret, L., Launeau, P., Diot, H., Sizaret, S., 2013. Magnetic and shape fabrics of magnetite in simple shear flows. J. Volcanol. Geotherm. Res. 249, 25–38.

Archanjo, C., Launeau, P., 2004. Magma flow inferred from preferred orientations of plagioclase of the Rio Ceará-Mirim dyke swarm (NE Brazil) and its AMS significance. Geol. Soc. Lond. Spec. Publ. 238 (1), 285–298.

Archanjo, C., Bouchez, J.-L., Corsini, M., Vauchez, A., 1994. The Pombal granite pluton: magnetic fabric, emplacement and relationships with the Brasiliano strike-slip set ting of NE Brazil (Paraiba State). J. Struct. Geol. 16 (3), 323–335.

Archanjo, C., Launeau, P., Bouchez, J.-L., 1995. Magnetic fabric vs. magnetite and biotite shape fabrics of the magnetite-bearing granite pluton of Gameleiras (Northeast Brazil). Phys. Earth Planet. Inter. 89 (1), 63–75.

Archanjo, C., Araújo, M., Launeau, P., 2002. Fabric of the Rio Ceará–Mirim mafic dike swarm (northeastern Brazil) determined by anisotropy of magnetic susceptibility and image analysis. J. Geophys. Res. 107 (B3), 1–13.

Archanjo, C., Launeau, P., Hollanda, M., Macedo, J., Liu, D., 2009. Scattering of magnetic fabrics in the Cambrian alkaline granite of Meruoca (Ceará state, northeastern Brazil). Int. J. Earth Sci. 98 (8), 1793–1807.

Archanjo, C., Campanha, G., Salazar, C., Launeau, P., 2012. Using AMS combined with mineral shape preferred orientation analysis to understand the emplacement fabrics of the Apiaí gabbro-norite (Ribeira Belt, SE Brazil). Int. J. Earth Sci. 101 (3), 731–745.

Baker, D.R., Mancini, L., Polacci, M., Higgins, M., Gualda, G., Hill, R., Rivers, M., 2012. An introduction to the application of X-ray microtomography to the three-dimensional study of igneous rocks. Lithos 148, 262–276.

Boiron, T., 2011. Étude multi-échelle des variations structurales, géochimiques et des propriétés magnétiques des coulées basaltiques prismées: exemple de la coulée de La Palisse (Ardèche) et de Saint-Arcons-d'Allier (Haute-Loire). Ecole Nationale Supérieure des Mines de Saint-Etienne, France (Ph.D. thesis).

Bouchez, J., 1997. Granite is never isotropic: an introduction to AMS studies of granitic rocks. In: Bouchez, J.L., Hutton, D.H.W., Stephens, W.E. (Eds.), Granite: From Segregation of Melt to Emplacement Fabrics vol. 8. Kluwer Academic Publishers, Dordrecht, pp. 95–112.

Brack, P., 1985. Multiple intrusions—examples from the Adamello batholith (Italy) and their significance on the mechanisms of intrusion. Mem. Soc. Geol. Ital. 26, 145–157.

Cañón-Tapia, E., 1996. Single-grain versus distribution anisotropy: a simple three-dimensional model. Phys. Earth Planet. Inter. 94 (1), 149–158.

Cañón-Tapia, E., 2001. Factors affecting the relative importance of shape and distribution anisotropy in rocks: theory and experiments. Tectonophysics 340 (1), 117–131.

Cañón-Tapia, E., 2004. Anisotropy of magnetic susceptibility of lava flows and dykes: a historical account. Geol. Soc. Lond. Spec. Publ. 238 (1), 205–225.

Cañón-Tapia, E., Chávez-Álvarez, J., 2004. Theoretical aspects of particle movement in flowing magma: implications for the anisotropy of magnetic susceptibility of dykes. Geol. Soc. Lond. Spec. Publ. 238 (1), 227–249.

Cañón-Tapia, E., Coe, R., 2002. Rock magnetic evidence of inflation of a flood basalt lava flow. Bull. Volcanol. 64 (5), 289–302.

Cruden, A., Tobisch, O., Launeau, P., 1999. Magnetic fabric evidence for conduit-fed emplacement of a tabular intrusion: Dinkey Creek Pluton, central Sierra Nevada batholith, California. J. Geophys. Res. 104 (B5), 10511–10530.

Diot, H., Bolle, O., Lambert, J., Launeau, P., Duchesne, J., 2003. The Tellnes ilmenite deposit (Rogaland, South Norway): magnetic and petrofabric evidence for emplacement of a Ti-enriched noritic crystal mush in a fracture zone. J. Struct. Geol. 25 (4), 481–501.

Eriksson, P., Riishuus, M., Sigmundsson, F., Elming, S., 2011. Magma flow directions inferred from field evidence and magnetic fabric studies of the Streitishvarf composite dike in east Iceland. J. Volcanol. Geotherm. Res. 206 (1–2), 30–45.

Feldkamp, L., Davis, L., Kress, J., 1984. Practical cone-beam algorithm. J. Opt. Soc. Am. 1 (6), 612–619.

Flinn, D., 1962. On folding during three-dimensional progressive deformation. Q. J. Geol. Soc. Lond. 118 (1–4), 385–428.

Floess, D., 2013. Contact metamorphism and emplacement of the western Adamello tonalite. (Ph.D. thesis). Université de Lausanne.

Gaillot, P., St Blanquat, M.d., Bouchez, J., 2006. Effects of magnetic interactions in anisotropy of magnetic susceptibility: models, experiments and implications for igneous rock fabrics quantification. Tectonophysics 418 (1), 3–19.

Geoffroy, L., Callot, J., Aubourg, C., Moreira, M., 2002. Magnetic and plagioclase linear fabric discrepancy in dykes: a new way to define the flow vector using magnetic foliation. Terra Nova 14 (3), 183–190.

Gleizes, G., Leblanc, D., Santana, V., Olivier, P., Bouchez, J., 1998. Sigmoidal structures featuring dextral shear during emplacement of the Hercynian granite complex of Cauterets-Panticosa (Pyrenees). J. Struct. Geol. 20 (9–10), 1229–1245.

Gountié Dedzo, M., Nédélec, A., Nono, A., Njanko, T., Font, E., Kamgang, P., Njonfang, E., Launeau, P., 2011. Magnetic fabrics of

the Miocene ignimbrites from West-Cameroon: implications for pyroclastic flow source and sedimentation. J. Volcanol. Geotherm. Res. 203 (3), 113–132.

Grégoire, V., de St Blanquat, M., Nédélec, A., Bouchez, J., 1995. Shape anisotropy versus magnetic interactions of magnetite grains: experiments and application to AMS in granitic rocks. Geophys. Res. Lett. 22 (20), 2765–2768.

Grégoire, V., Darrozes, J., Gaillot, P., Nédélec, A., Launeau, P., 1998. Magnetite grain shape fabric and distribution anisotropy vs rock magnetic fabric: a three-dimensional case study. J. Struct. Geol. 20 (7), 937–944.

Hargraves, R., Johnson, D., Chan, C., 1991. Distribution anisotropy: the cause of AMS in igneous rocks? Geophys. Res. Lett. 18 (12), 2193–2196.

Hrouda, F., Ježek, J., 1999. Theoretical models for the relationship between magnetic anisotropy and strain: effect of triaxial magnetic grains. Tectonophysics 301 (3), 183–190.

Hrouda, F., Táborská, S., Schulmann, K., Ježek, J., Dolejš, D., 1999. Magnetic fabric and rhe ology of co-mingled magmas in the Nasavrky Plutonic Com plex (E Bohemia): impli cations for intrusive strain regime and emplacement mechanism. Tectonophysics 307 (1–2), 93–111.

Jelinek, V., 1981. Characterization of the magnetic fabric of rocks. Tectonophysics 79 (3–4), T63–T67.

John, B., Blundy, J., 1993. Emplacement-related deformation of granitoid magmas, southern Adamello Massif, Italy. Geol. Soc. Am. Bull. 105 (12), 1517–1541.

John, B., Stünitz, H., 1997. Magmatic fracturing and small-scale melt segregation during pluton emplacement: evidence from the Adamello massif (Italy). In: Bouchez, J.L., Hutton, D.H.W., Stephens, W.E. (Eds.), Granite: From Segregation of Melt to Emplacement Fabrics vol. 8. Kluwer Academic Publishers, Dordrecht, pp. 55–74.

Ketcham, R., 2005a. Three-dimensional grain fabric measurements using high- resolution X-ray computed tomography. J. Struct. Geol. 27 (7), 1217–1228.

Ketcham, R.A., 2005b. Computational methods for quantitative analysis of three-dimensional features in geological specimens. Geosphere 1 (1), 32–41.

Launeau, P., Cruden, A., 1998. Magmatic fabric acquisition mechanisms in a syenite: results of a combined anisotropy of magnetic susceptibility and image analysis study. J. Geophys. Res. 103 (B3), 5067–5089.

Launeau, P., Robin, P., 2005. Determination of fabric and strain ellipsoids from measured sectional ellipses – implementation and applications. J. Struct. Geol. 27 (12), 2223–2233.

Launeau, P., Archanjo, C., Picard, D., Arbaret, L., Robin, P., 2010. Two- and three-dimensional shape fabric analysis by the intercept method in grey levels. Tectonophysics 492 (1–4), 230–239.

Loock, S., Diot, H., Wyk, Van, de Vries, B., Launeau, P., Merle, O., Vadeboin, F., Petronis, M., 2008. Lava flow internal structure found from AMS and textural data: an example in methodology from the Chaîne des Puys, France. J. Volcanol. Geotherm. Res. 177 (4), 1092–1104.

López de Luchi, M., Rapalini, A., Siegesmund, S., Steenken, A., 2004. Application of magnetic fabrics to the emplacement and tectonic history of Devonian granitoids in central Argentina. Geol. Soc. Lond. Spec. Publ. 238 (1), 447–474.

O'Reilly, W., 1984. Rock and Mineral Magnetism. Blackie, Glasgow.

Petronis, M., Hacker, D., Holm, D., Geissman, J., Harlan, S., 2004. Magmatic flow paths and palaeomagnetism of the Miocene Stoddard Mountain laccolith, Iron Axis region, Southwestern Utah, USA. Geol. Soc. Lond. Spec. Publ. 238 (1), 251–283.

Petronis, M., O'Driscoll, B., Stevenson, C., Reavy, R., 2012. Controls on emplacement of the Caledonian Ross of Mull Granite, NW Scotland: anisotropy of magnetic susceptibility and magmatic and regional structures. Geol. Soc. Am. Bull. 124 (5–6), 906–927.

Raposo, M., Pressi, L., de Assis Janasi, V., 2012. Magnetic fabrics and their relationship with the emplacement of the Piracaia pluton, SE Brazil. Int. J. Earth Sci. 101 (3), 773–786.

Robin, P., 2002. Determination of fabric and strain ellipsoids from measured sectional ellipses – theory. J. Struct. Geol. 24 (3), 531–544.

Rochette, P., 1987. Magnetic susceptibility of the rock matrix related to magnetic fabric studies. J. Struct. Geol. 9 (8), 1015–1020.

Rochette, P., Aubourg, C., Perrin, M., 1999. Is this magnetic fabric normal? A review and case studies in volcanic formations. Tectonophysics 307 (1–2), 219–234.

Schöpa, A., St Blanquat, M.d., Blundy, J., Annen, C., Launeau, P., Brack, P., 2014. Emplacement of the Lago della Vacca Complex, southern Adamello Batholith: a combined AMS and petrofabric study. J. Struct. Geol. 1–82 (submitted for publication).

St Blanquat, M.d., Law, R., Bouchez, J., Morgan, S., 2001. Internal structure and emplacement of the Papoose Flat pluton: an integrated structural, petrographic, and magnetic susceptibility study. Geol. Soc. Am. Bull. 113 (8), 976–995.

St Blanquat, M.d., Habert, G., Horsman, E., Morgan, S., Tikoff, B., Launeau, P., Gleizes, G., 2006. Mechanisms and duration of non-tectonically assisted magma emplacement in the upper crust: the Black Mesa pluton, Henry Mountains, Utah. Tectonophysics 428 (1-4), 1–31.

Stephenson, A., 1994. Distribution anisotropy: two simple models for magnetic lineation and foliation. Phys. Earth Planet. Inter. 82 (1), 49–53.

Ulmer, P., Callegari, E., Sonderegger, U., 1985. Genesis of the mafic and ultra-mafic rocks and their genetical relations to the tonalitic-trondhjemitic granitoids of the southern part of the Adamello batholith (Northern Italy). Mem. Soc. Geol. Ital. 26, 171–222.

Woodcock, N., 1977. Specification of fabric shapes using an eigenvalue method. Geol. Soc. Am. Bull. 88 (9), 1231–1236.

Figures

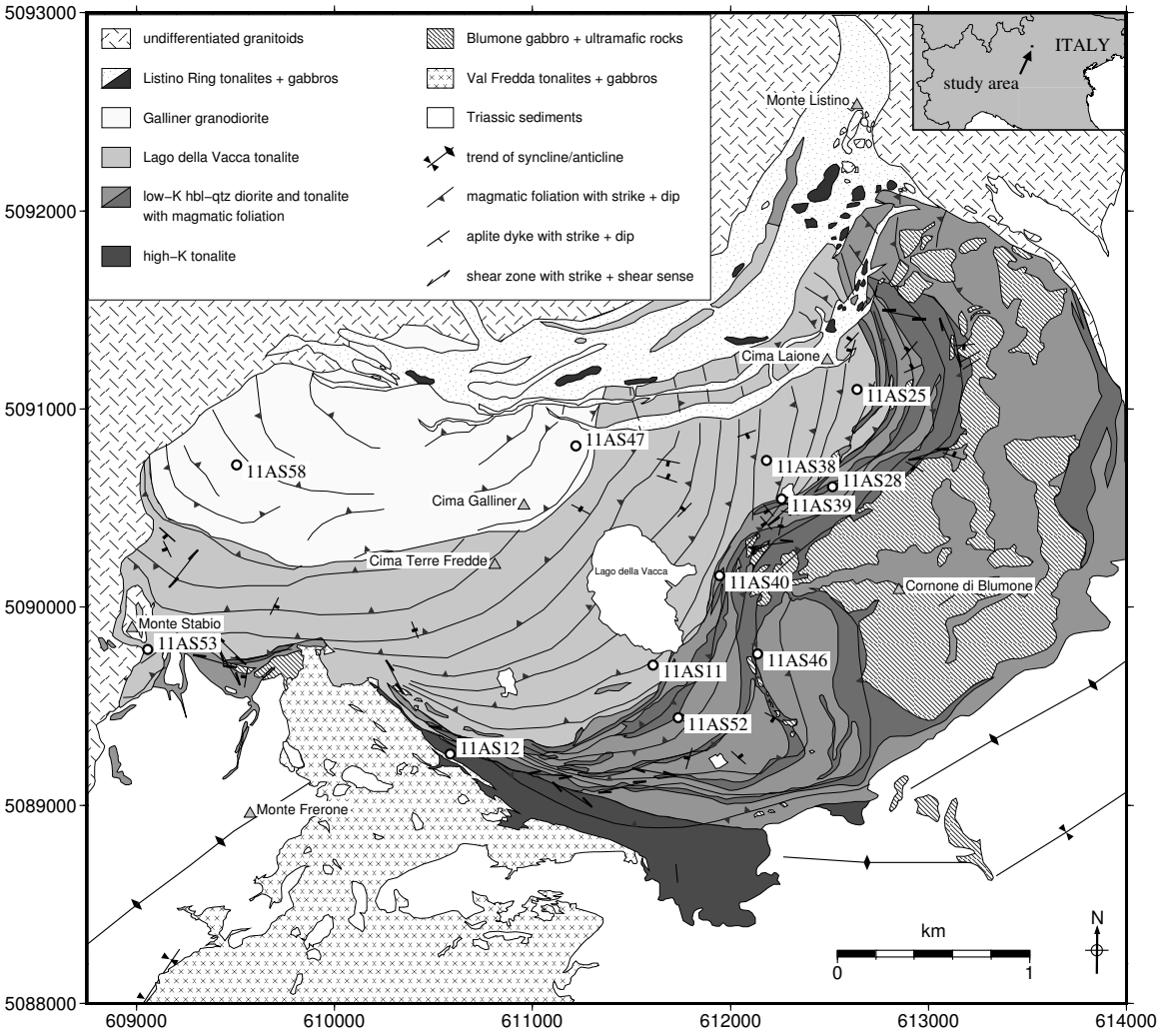

Fig. 1. Sample locations in the Lago della Vacca Complex (LVC). Geological map after John and Blundy (1993), Brack (1985) and Ulmer et al. (1985).

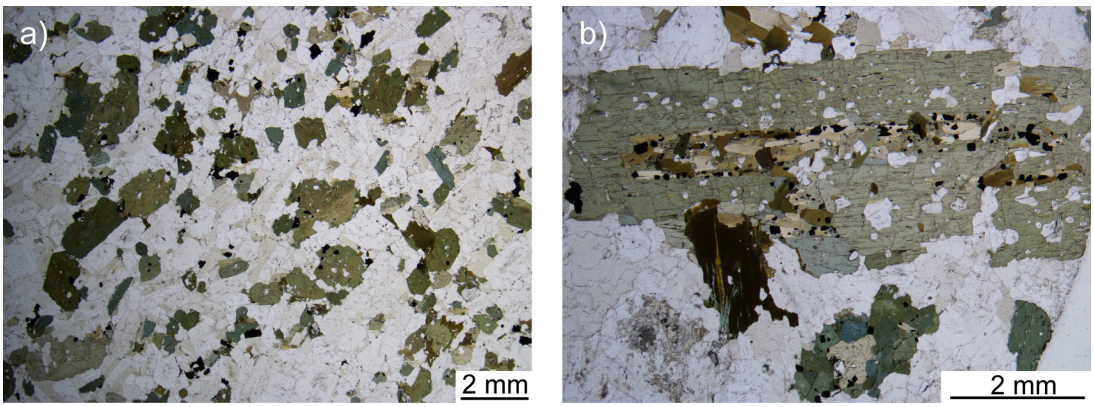

Fig. 2. Microphotographs of Lago della Vacca tonalite. a) Hornblende, plagioclase and quartz crystals, defining the macroscopic fabric as measured in the field and determined with IA, with interstitial oxides (opaque grains). b) Large hornblende crystal with oriented inclusions of oxides. Oxides are present as single grains or clusters of grains.

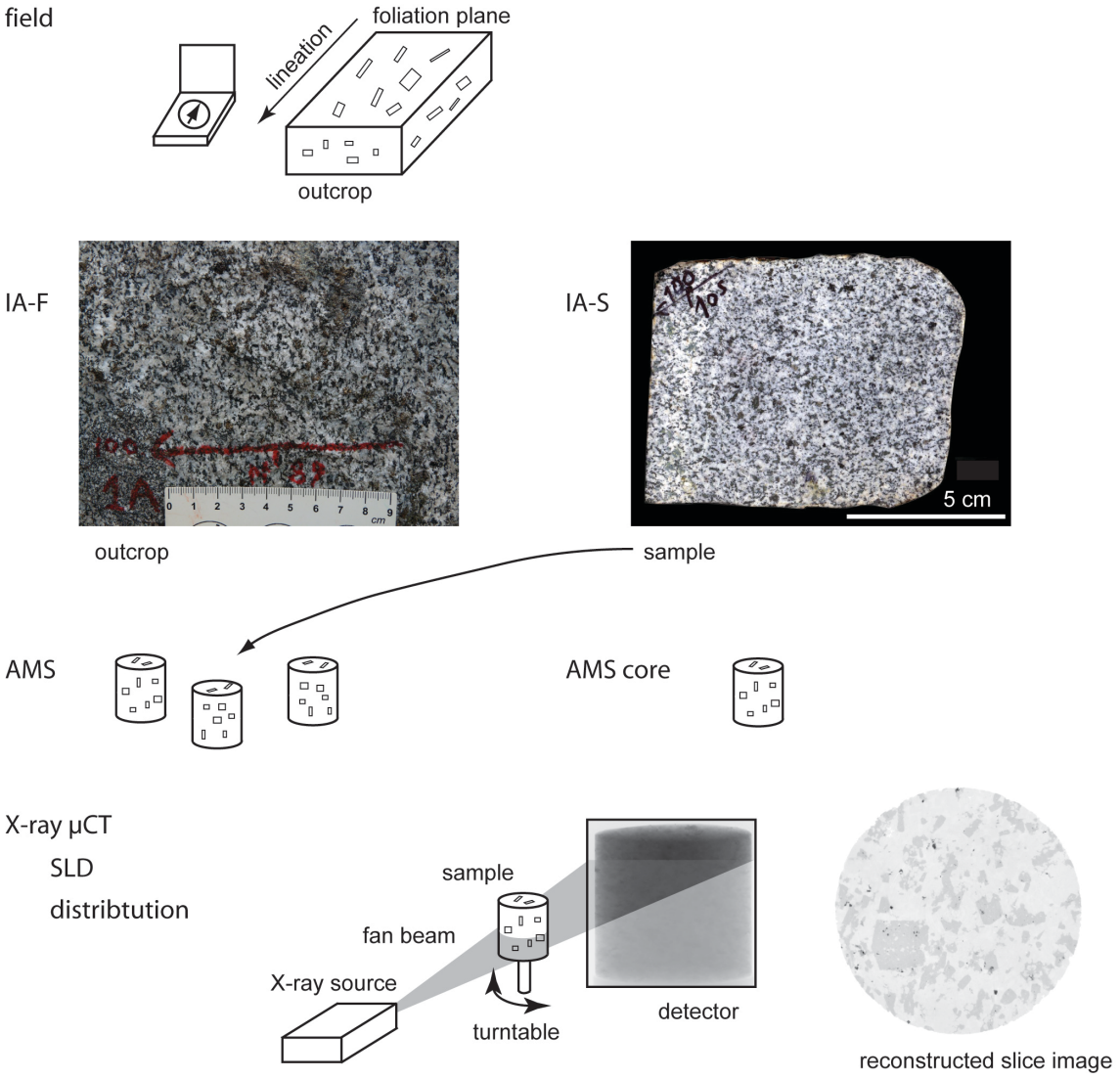

Fig. 3. Different methods to measure fabrics at outcrops, of a sample and of core specimens. IA-F: Image analysis (IA) of rock surface photographs taken in the field; IA-S: IA of rock sample images; SLD: star length distribution.

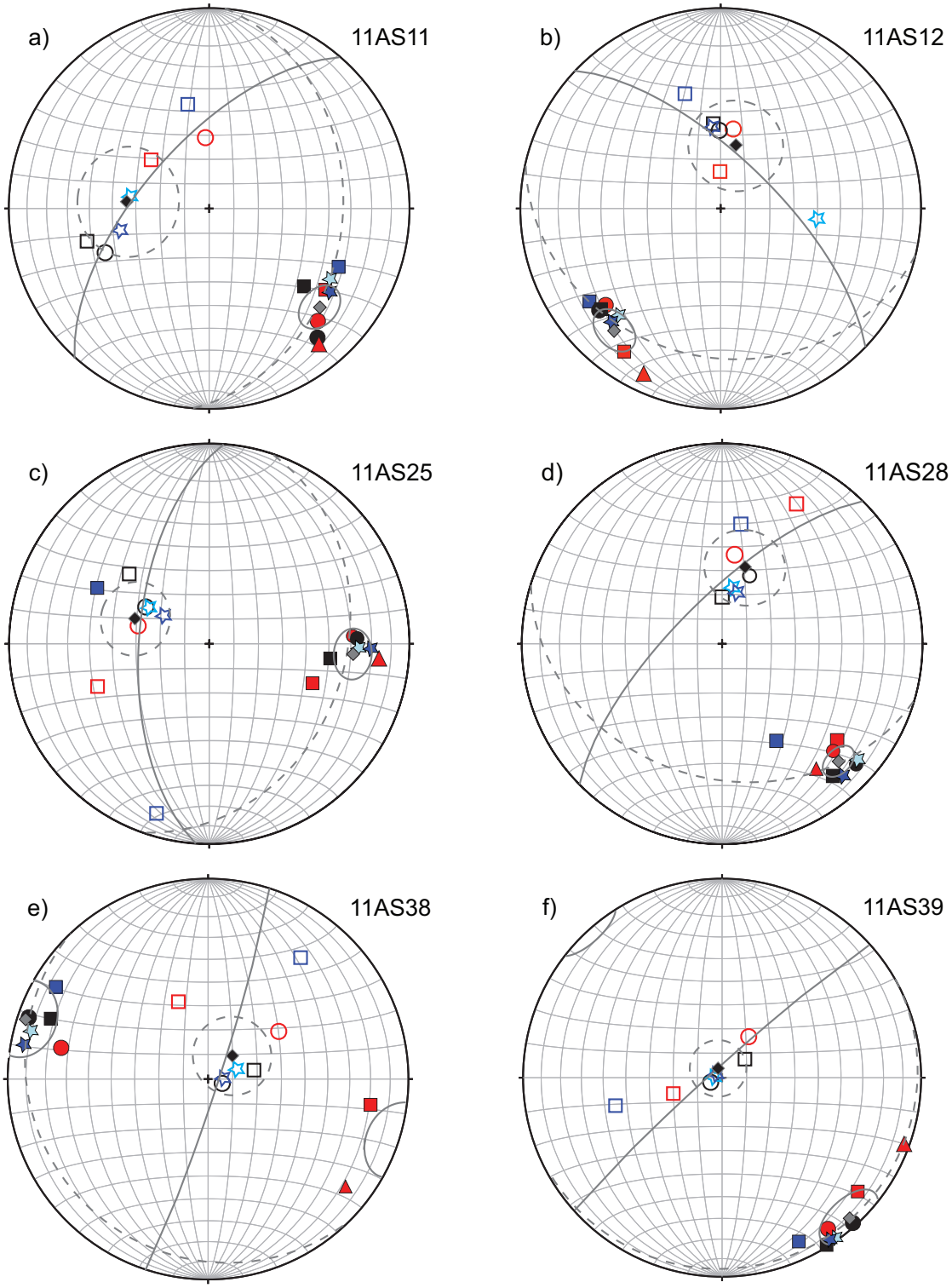
a)
11AS11
b)
11AS12
c)
11AS25
d)
11AS28
e)
11AS38
f)
11AS39

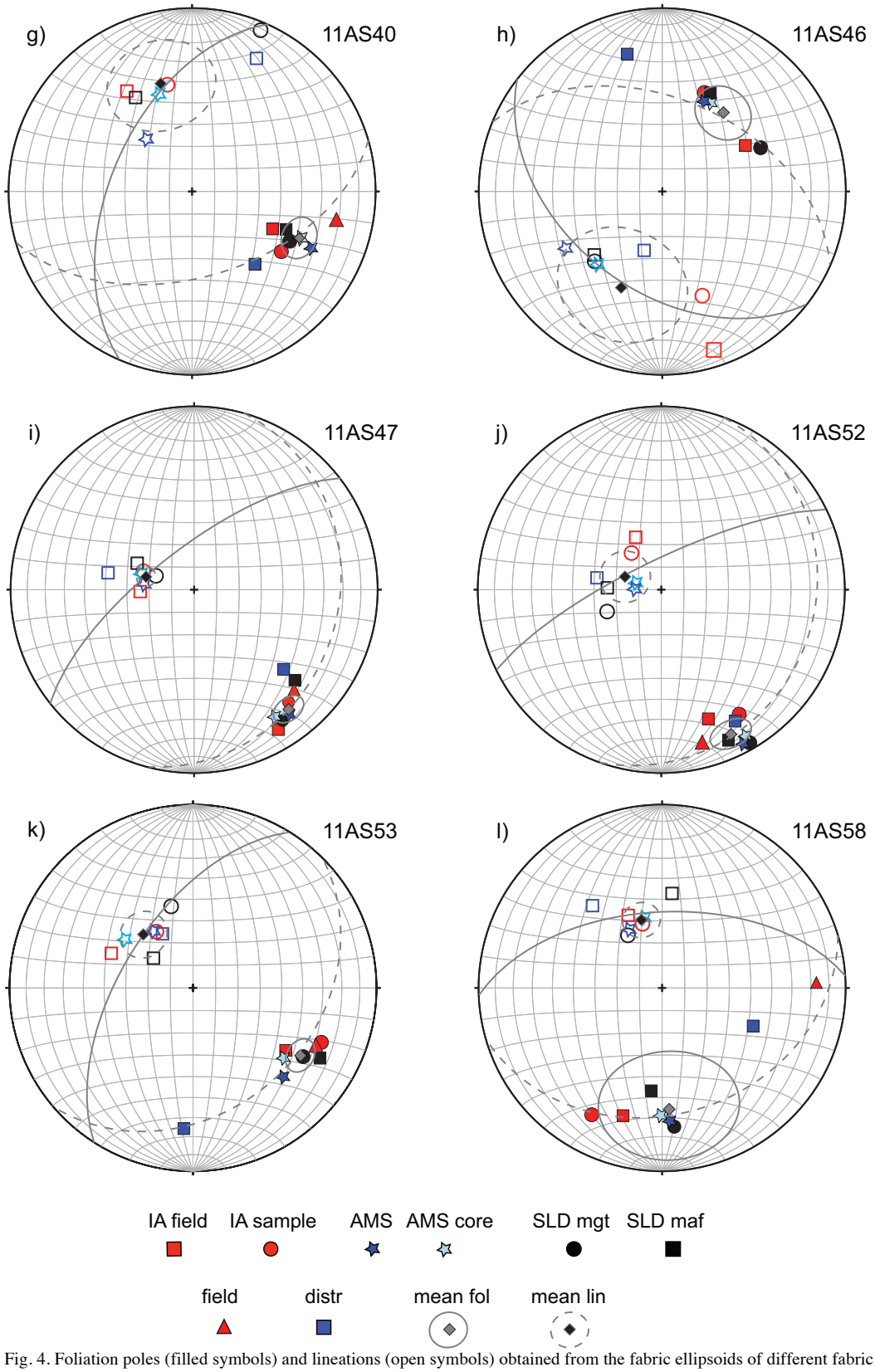

Fig. 4. Foliation poles (filled symbols) and lineations (open symbols) obtained from the fabric ellipsoids of different fabric measurements, lower hemisphere, equal area projection. Grey diamond is the mean foliation vector (equivalent great circle in solid grey) and black diamond is the mean lineation vector (equivalent great circle in broken grey), both with 95% confidence cone. Sample number is given in the upper right corner of each subfigure. See Fig. 3 for explanation of abbreviations. mgt: magnetite; maf: mafic silicates.

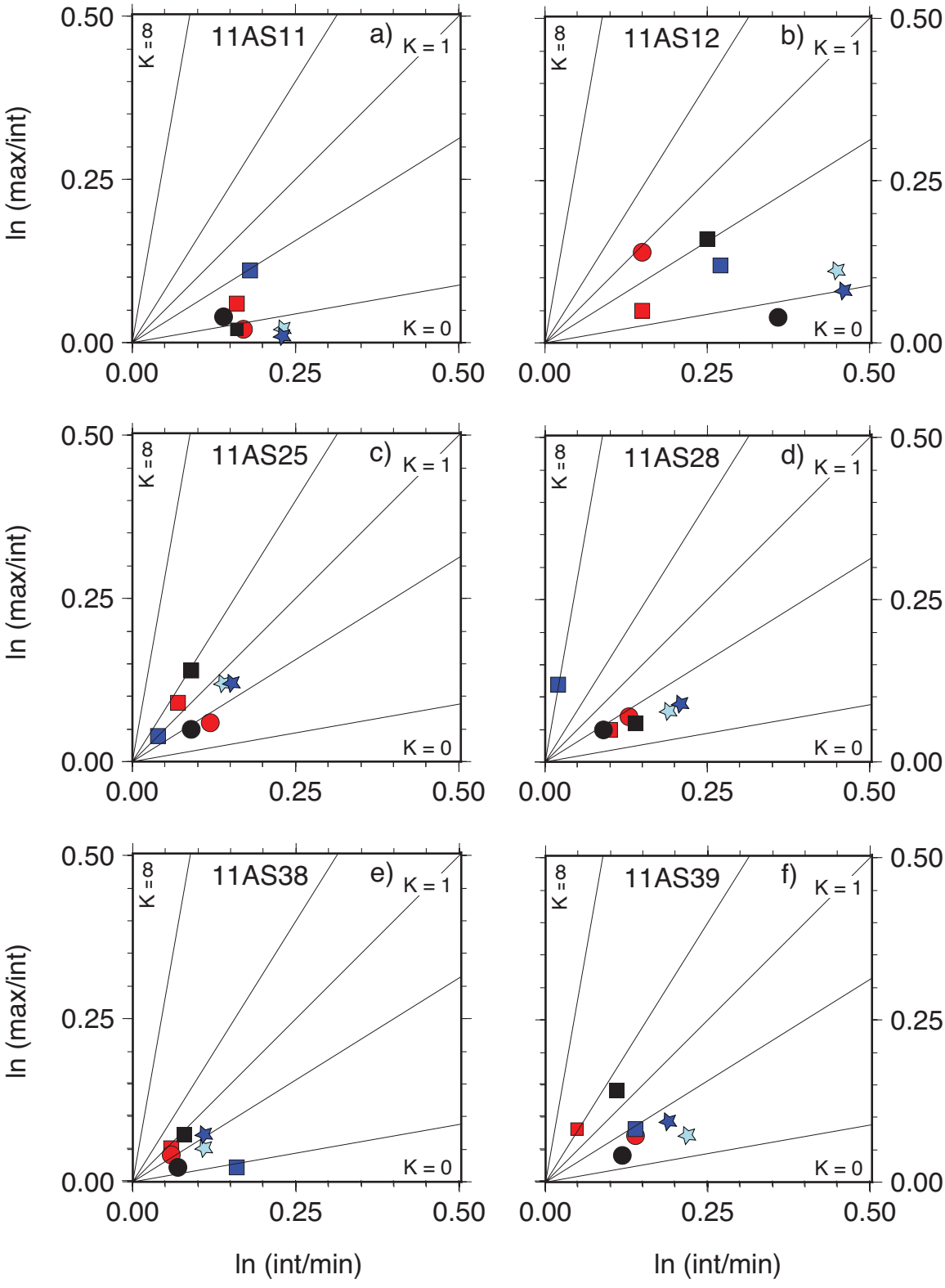
11AS11
a)
11AS12
b)
11AS25
c)
11AS28
d)
11AS38
e)
11AS39
f)
K = ∞
K = 1
K = 0
0.00
0.25
0.50
ln (max/int)
ln (int/min)

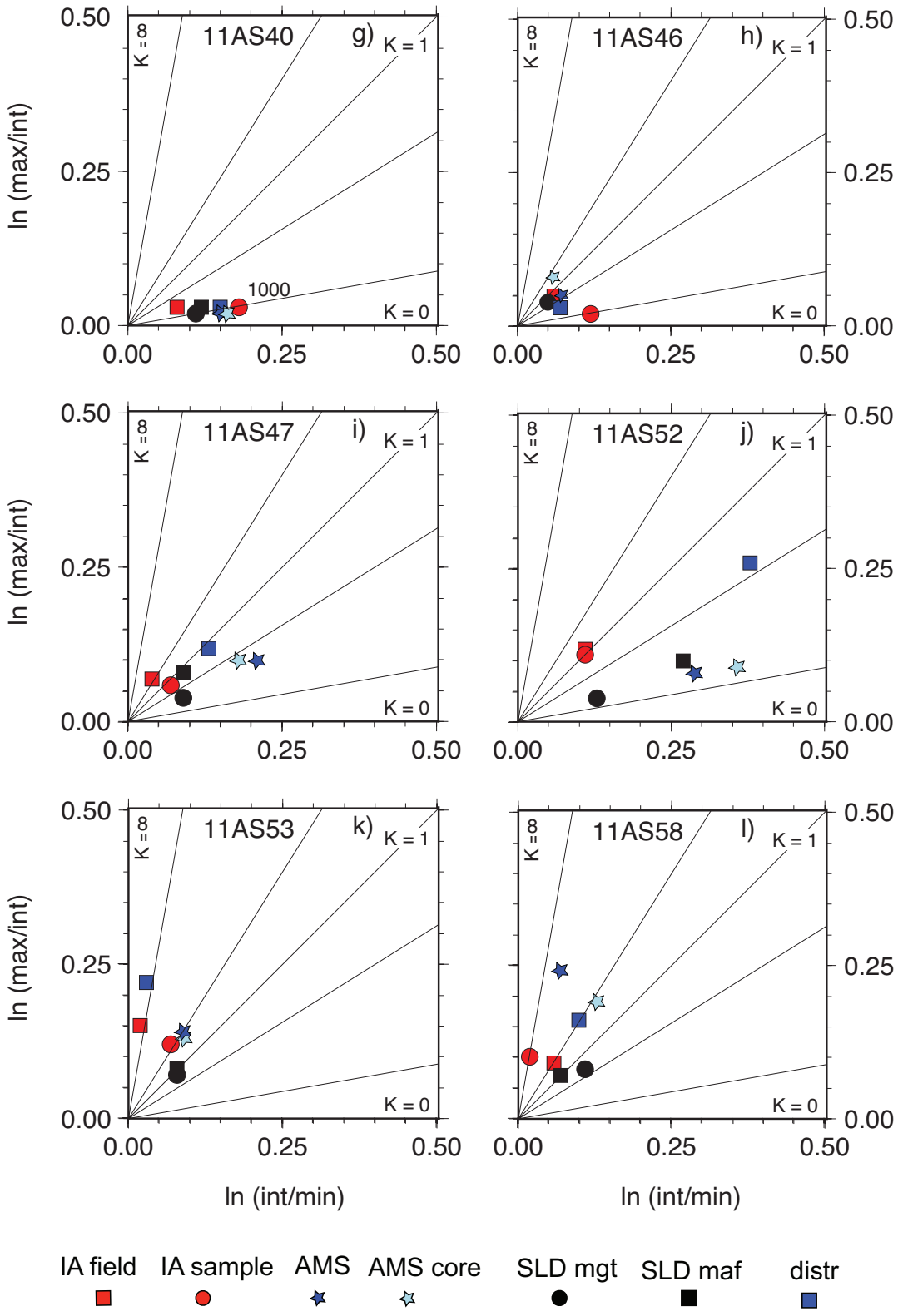

Fig. 5. Flinn-type diagrams for axial ratios of the fabric ellipsoids. See Fig. 3 for explanation of abbreviations. mgt: magnetite; maf: mafic silicates.

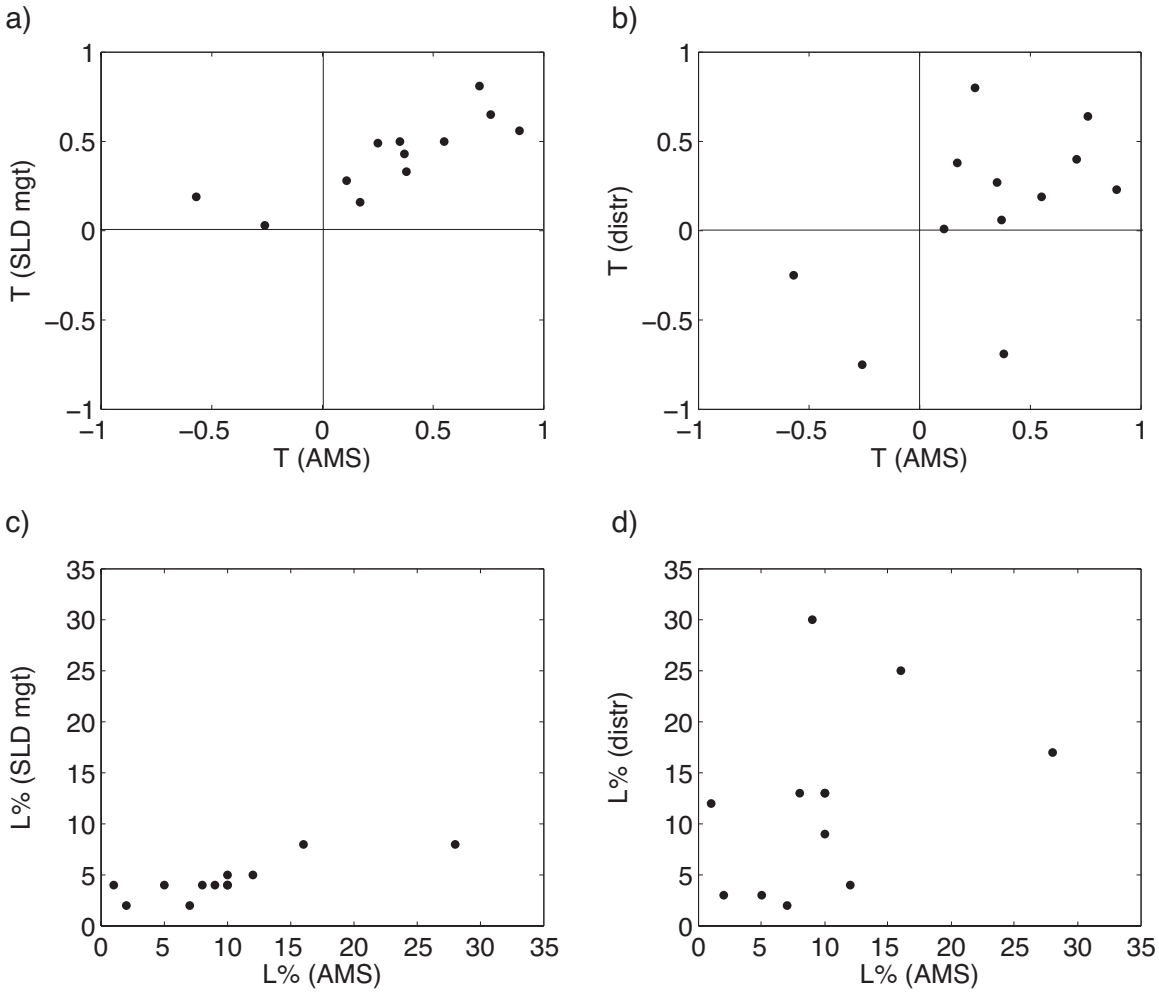

Fig. 6. Shape parameter T of the fabric ellipsoids of a) AMS and magnetite SLD, and b) AMS and distribution anisotropy. Linear anisotropy L% of the fabric ellipsoids of c) AMS and magnetite SLD, and d) AMS and distribution anisotropy.

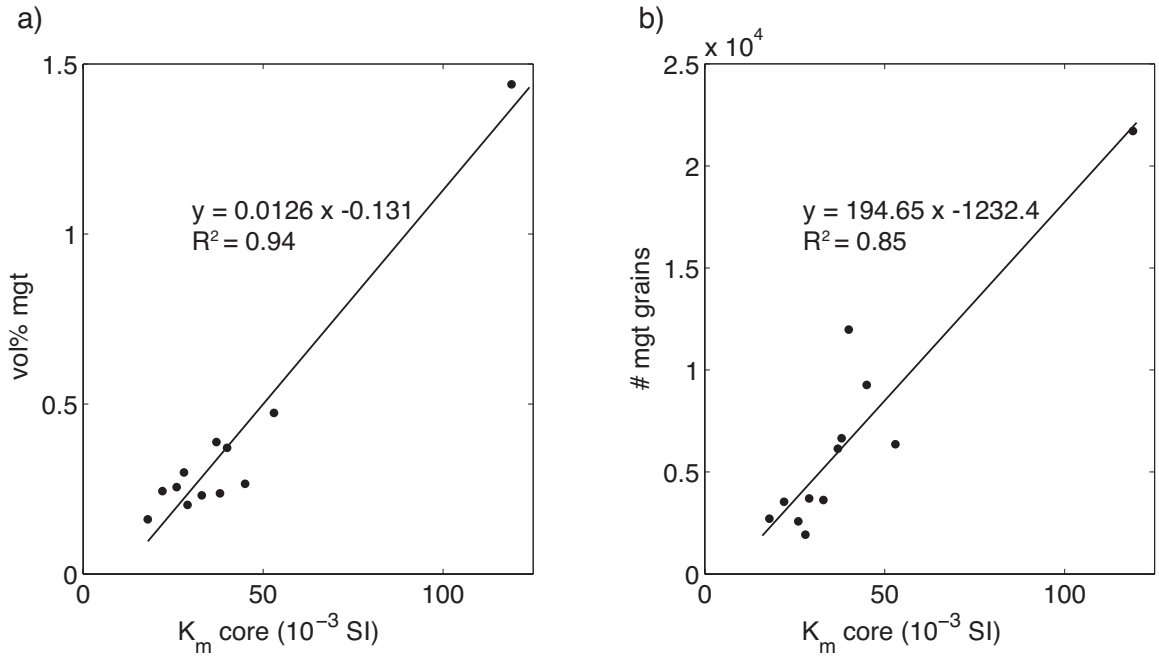

Fig. 7. Relation of the mean susceptibility K_m of the AMS sample core and a) the vol% of magnetite, and b) the number of magnetite grains in the samples.

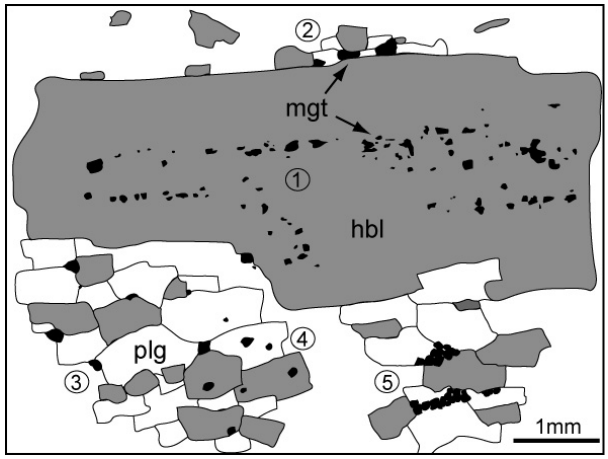

Fig. 8. Generic drawing of magnetite (mgt) microstructures. 1) Magnetite inclusions parallel to outline of large hornblende (hbl) host, 2) magnetites tracing the shape of hornblende, 3) interstitial magnetites, 4) magnetite inclusions in hornblende and plagioclase (plg), 5) magnetite clusters. In the granitoid samples, the long axes of the magnetites are usually parallel to the long axes of hornblendes and plagioclases.

Tables

Table 1. Comparison of the fabric measurement techniques.

Technique	Mineral(s)	Area/volume analysed	Pixel size (μm)
Field	hornblende, biotite	outcrop	–
IA field	main silicates	$3 \times 40–250\ cm^3$	58
IA sample	main silicates	$3 \times 24–80\ cm^3$	58
AMS	magnetite	6–9 cores à $10.8\ cm^3$	–
AMS core	magnetite	1 core à $10.8\ cm^3$	–
SLD mgt	oxides	$10.8\ cm^3$	23
SLD maf	hornblende, biotite	$10.8\ cm^3$	23
Distribution	oxides	$10.8\ cm^3$	23

Table 2. Results of the different fabric measurement techniques. K_m is the mean susceptibility in 10^{-3} SI. (int/min) and (max/int) are the axial ratios of the fabric ellipsoids.

Sample	Method	Foliation			Lineation		ln (int/min)	ln (max/int)
K_m		Strike	Dip dir	Dip	Trend	Plunge		
11AS11	field	231	N	76				
	IA field	215	W	60	310	59	0.16	0.06
	IA sample	226	N	67	357	61	0.17	0.02
31	AMS	215	W	63	256	52	0.23	0.01
33	AMS core	210	W	59	279	57	0.23	0.02
	SLD mgt	230	W	73	247	43	0.14	0.04
	SLD maf	220	W	52	255	37	0.16	0.02
	MIL mgt	348	E	17	58	17	0.05	0.08
	MIL maf	228	W	57	44	6	0.08	0.09
	distr: 500	209	W	48	340	40	0.24	0.23
	distr: 700	196	W	64	349	41	0.17	0.13
	distr:1000	204	W	60	348	46	0.18	0.11
	distr: 1200	211	W	53	343	45	0.13	0.12
	distr: 1500	214	W	54	345	46	0.14	0.10
	IA refl	210	NW	47	311	46	0.10	0.02
	IA SEM	209	NE	59	243	59	0.17	0.02
	IA SEM mgt	223	NW	58	331	56	0.38	0.04
11AS12	field	295	N	80				
	IA field	304	N	75	359	75	0.15	0.05
	IA sample	320	N	64	9	57	0.15	0.14
27	AMS	315	E	67	354	56	0.46	0.08
22	AMS core	313	NE	63	96	50	0.45	0.11
	SLD mgt	320	E	68	359	58	0.36	0.04
	SLD maf	320	E	67	355	55	0.25	0.16
	MIL mgt	296	N	54	73	27	0.01	0.07
	MIL maf	248	W	71	25	63	0.01	0.06
	distr: 500	326	E	65	340	26	0.18	0.21
	distr: 700	325	E	63	343	31	0.29	0.13
	distr:1000	325	E	69	343	40	0.27	0.12
	distr: 1200	327	E	71	346	43	0.30	0.07
	distr: 1500	327	E	73	358	59	0.25	0.04
	IA refl	319	NE	63	355	49	0.18	0.05
	IA SEM	188	W	88	5	55	0.01	0.07
	IA SEM mgt	314	NE	79	126	32	0.12	0.08
11AS25	field	185	W	74				
	IA field	201	W	46	249	40	0.07	0.09
	IA sample	177	W	61	284	60	0.12	0.06
40	AMS	182	W	70	301	68	0.15	0.12
40	AMS core	182	W	64	301	61	0.14	0.12
	SLD mgt	178	W	63	300	60	0.09	0.05
	SLD maf	187	W	51	311	46	0.09	0.14
	MIL mgt	327	E	78	337	43	0.09	0.09
	MIL maf	208	W	46	24	4	0.15	0.05
	distr: 500	183	W	34	180	86	0.03	0.08
	distr: 700	183	W	35	48	45	0.04	0.10
	distr:1000	197	W	12	27	53	0.04	0.04
	distr: 1200	56	S	39	39	70	0.03	0.04
	distr: 1500	208	W	11	34	56	0.02	0.02
11AS28	field	233	N	67				
	IA field	220	W	64	28	22	0.10	0.05
	IA sample	224	W	66	8	53	0.13	0.07
44	AMS	228	W	78	17	68	0.21	0.09
45	AMS core	220	NW	78	11	66	0.19	0.08
	SLD mgt	222	W	79	22	60	0.09	0.05
	SLD maf	230	NW	75	360	71	0.14	0.06
	MIL mgt	139	S	49	219	49	0.05	0.09
	MIL maf	230	W	80	20	70	0.12	0.09
	distr: 500	257	N	58	359	57	0.12	0.12
	distr: 700	240	NW	58	20	46	0.06	0.16
	distr:1000	241	NW	46	9	39	0.02	0.12
	distr: 1200	218	W	64	18	37	0.03	0.10
	distr: 1500	212	W	70	13	42	0.05	0.10
11AS38	field	218	W	76				
	IA field	189	W	71	339	56	0.06	0.05
	IA sample	12	E	64	56	55	0.06	0.04
30	AMS	10	E	83	89	83	0.11	0.07
29	AMS core	15	E	80	69	77	0.11	0.05
	SLD mgt	19	E	84	107	84	0.07	0.02
	SLD maf	21	E	73	79	71	0.08	0.07
	MIL mgt	169	W	8	229	7	0.06	0.09
	MIL maf	25	E	86	200	57	0.10	0.03
	distr: 500	190	W	75	1	32	0.25	0.04
	distr: 700	202	W	89	22	13	0.16	0.04

(continued on next page)

Table 2 (*continued*)

Sample	Method	Foliation			Lineation		ln (int/min)	ln (max/int)
K_m		Strike	Dip dir	Dip	Trend	Plunge		
	distr:1000	31	E	78	37	25	0.16	0.02
	distr: 1200	25	E	82	31	38	0.12	0.04
	distr: 1500	26	E	69	32	13	0.09	0.08
11AS39	field	200	W	87				
	IA field	220	W	78	252	69	0.05	0.08
	IA sample	235	W	82	33	70	0.14	0.07
34	AMS	237	W	88	297	88	0.19	0.09
37	AMS core	235	NW	88	262	87	0.22	0.07
	SLD mgt	228	NW	88	248	85	0.12	0.04
	SLD maf	238	NW	89	51	78	0.11	0.14
	MIL mgt	157	W	47	209	41	0.05	0.08
	MIL maf	94	S	74	271	79	0.14	0.08
	distr: 500	100	S	82	266	59	0.07	0.14
	distr: 700	251	N	84	260	59	0.05	0.13
	distr:1000	245	N	80	255	44	0.14	0.08
	distr: 1200	248	N	82	259	52	0.13	0.10
	distr: 1500	250	N	85	256	52	0.12	0.08
11AS40	field	191	W	69				
	IA field	205	W	40	327	35	0.08	0.03
	IA sample	214	W	49	347	40	0.18	0.03
52	AMS	206	W	61	320	59	0.15	0.02
53	AMS core	204	W	55	342	43	0.16	0.02
	SLD mgt	207	W	50	23	5	0.11	0.02
	SLD maf	202	W	46	329	40	0.12	0.03
	MIL mgt	21	E	68	35	32	0.08	0.09
	MIL maf	239	W	51	35	27	0.09	0.02
	distr: 500	239	W	48	247	8	0.13	0.07
	distr: 700	219	W	50	228	11	0.11	0.08
	distr:1000	229	W	44	26	21	0.15	0.03
	distr: 1200	235	W	38	336	38	0.14	0.01
	distr: 1500	243	W	35	259	11	0.13	0.05
11AS46	IA field	151	W	43	162	10	0.06	0.05
	IA sample	113	S	49	159	39	0.12	0.02
108	AMS	115	S	45	239	39	0.07	0.05
119	AMS core	119	S	46	221	46	0.06	0.08
	SLD mgt	156	S	49	224	46	0.05	0.04
	SLD maf	116	S	50	227	48	0.07	0.03
	MIL mgt	89	S	45	231	32	0.08	0.10
	MIL maf	161	W	47	281	43	0.04	0.10
	distr: 500	62	S	77	226	51	0.04	0.14
	distr: 700	75	S	67	214	57	0.07	0.08
	distr:1000	76	S	66	197	63	0.07	0.03
	distr: 1200	75	S	68	178	68	0.05	0.04
	distr: 1500	81	S	70	197	67	0.03	0.06
	IA refl	109	S	59	159	52	0.06	0.04
	IA SEM	147	SW	69	297	53	0.10	0.05
	IA SEM mgt	106	S	35	151	27	0.04	0.02
11AS47	field	225	N	66				
	IA field	239	N	78	268	66	0.04	0.07
	IA sample	230	N	69	290	66	0.07	0.06
23	AMS	233	W	75	277	68	0.21	0.10
26	AMS core	238	NW	71	287	66	0.18	0.10
	SLD mgt	236	W	75	290	72	0.09	0.04
	SLD maf	222	W	63	295	62	0.09	0.08
	MIL mgt	118	S	27	226	26	0.08	0.07
	MIL maf	212	S	67	247	54	0.09	0.06
	distr: 500	180	W	45	288	44	0.05	0.24
	distr: 700	199	W	45	291	45	0.12	0.19
	distr:1000	222	W	55	281	51	0.13	0.12
	distr: 1200	227	W	58	283	53	0.17	0.11
	distr: 1500	222	W	57	272	50	0.12	0.12
	IA refl	282	N	77	307	61	0.03	0.04
	IA SEM	186	W	71	291	70	0.12	0.19
	IA SEM mgt	226	NW	69	233	19	0.04	0.05
11AS52	field	255	N	75				
	IA field	250	N	64	334	64	0.11	0.12
	IA sample	238	N	69	321	69	0.11	0.11
36	AMS	241	N	84	272	79	0.29	0.08
38	AMS core	240	NW	82	287	79	0.36	0.09
	SLD mgt	240	W	86	248	64	0.13	0.04
	SLD maf	246	W	79	272	66	0.27	0.10
	MIL mgt	29	E	57	40	16	0.07	0.08
	MIL maf	249	W	74	253	12	0.26	0.02
	distr: 500	235	W	73	268	61	0.53	0.30
	distr: 700	240	W	72	279	63	0.42	0.29

Table 2 (*continued*)

Sample	Method	Foliation			Lineation		ln (int/min)	ln (max/int)
K_m		Strike	Dip dir	Dip	Trend	Plunge		
	distr:1000	241	W	71	281	61	0.38	0.26
	distr: 1200	236	W	73	270	60	0.39	0.18
	distr: 1500	238	W	73	263	56	0.35	0.15
11AS53	field	205	W	63				
	IA field	214	W	51	293	50	0.02	0.15
	IA sample	203	W	65	327	60	0.07	0.12
9	AMS	225	W	59	325	59	0.09	0.14
18	AMS core	217	NW	52	305	53	0.09	0.13
	SLD mgt	212	W	60	345	52	0.08	0.07
	SLD maf	209	W	68	307	68	0.08	0.08
	MIL mgt	243	W	33	47	10	0.11	0.08
	MIL maf	183	W	56	211	27	0.04	0.08
	distr: 500	175	W	69	325	52	0.05	0.47
	distr: 700	282	N	67	323	57	0.05	0.28
	distr:1000	274	W	66	331	62	0.03	0.22
	distr: 1200	225	W	61	330	60	0.03	0.26
	distr: 1500	237	W	59	323	59	0.04	0.19
11AS58	field	178	N	73				
	IA field	287	N	62	335	54	0.06	0.09
	IA sample	299	N	68	343	60	0.02	0.10
33	AMS	267	N	62	331	60	0.07	0.24
28	AMS core	271	N	59	346	58	0.13	0.19
	SLD mgt	265	N	65	327	62	0.11	0.08
	SLD maf	276	N	47	6	47	0.07	0.07
	MIL mgt	133	S	27	223	27	0.05	0.10
	MIL maf	221	W	63	341	60	0.03	0.06
	distr: 500	152	W	81	330	10	0.13	0.20
	distr: 700	173	W	54	328	31	0.17	0.08
	distr:1000	203	W	45	320	41	0.10	0.16
	distr: 1200	212	W	48	325	46	0.14	0.14
	distr: 1500	205	W	46	317	44	0.06	0.20

Table 3. Intensive parameters P% = 100(max/min – 1), F% = 100(max/int – 1), L% = 100(int/min – 1) and shape parameter T = (2(ln int – ln min))/(ln max – ln min) – 1 of the different fabric measurement techniques. Sample lithologies include: Lago della Vacca tonalite (V), Galliner granodiorite (G), marginal units of high-K tonalites and low-K tonalites (M).

Site	Elevation (m a.s.l.)		AMS					All clustering	AMS core						IA samples				IA field			
		Unit	K_m (10^{-3}SI)	P%	F%	L%	shape T		Core	K_m (10^{-3}SI)	P%	F%	L%	shape T	P%	F%	L%	shape T	P%	F%	L%	shape T
11AS11b	2361	V	31	28	26	1	0.89	S>L	11AS11B	33	28	26	3	0.86	21	19	2	0.80	25	17	6	0.40
11AS12	2335	M	27	72	59	8	0.71	S>L	11AS12B	22	76	58	11	0.62	34	17	15	0.10	24	16	8	0.40
11AS25	2693	V	40	30	16	12	0.11	bad	11AS25C	40	29	15	12	0.10	20	13	6	0.30	18	7	10	-0.10
11AS28	2633	M	44	35	23	10	0.38	S=L	11AS28A	45	32	21	9	0.38	22	13	7	0.30	19	11	7	0.30
11AS38	2570	V	30	19	12	7	0.25	S=L	11AS38A	29	17	12	5	0.36	10	6	4	0.20	12	6	5	0.10
11AS39	2554	V	34	33	21	10	0.35	S=L	11AS39B	37	33	24	7	0.52	24	15	8	0.30	14	5	8	-0.20
11AS40b	2426	M	52	18	16	2	0.76	S>L	11AS40A	53	19	17	2	0.81	23	19	3	0.70	10	8	3	0.50
11AS46b	2354	M	108	13	8	5	0.17	bad	11AS46G	119	15	6	8	−0.13	15	13	2	0.80	11	6	5	0.10
11AS47	2459	G	23	35	23	10	0.37	S=L	11AS47A	26	33	20	11	0.26	14	7	7	0.00	12	4	8	-0.30
11AS52	2286	M	36	45	33	9	0.55	S=L	11AS52A	38	58	43	10	0.59	40	25	12	0.30	26	12	13	-0.10
11AS53	2497	V	19	26	9	16	−0.26	L>S	11AS53B	18	25	9	14	−0.19	21	7	13	−0.30	18	2	16	−0.70
11AS58	2090	G	33	36	7	28	−0.57	L>S	11AS58A	28	37	13	21	−0.20	13	2	10	−0.70	16	6	9	−0.20

Table 3 (*continued*)

Site	SLD mgt				SLD maf				distr (N = 1000 grains)				Mean fol vector				Mean lin vector				Dominance
	P%	F%	L%	shape T	P%	F%	L%	shape T	P%	F%	L%	shape T	Strike	Dip dir	Dip	95% conf cone	Strike	Dip dir	Dip	95% conf cone	
11AS11b	19	15	4	0.56	20	17	2	0.78	33	19	12	0.23	221	NW	64	8.38	5	E	33	21.44	**fol**
11AS12	49	44	4	0.81	51	28	18	0.20	48	32	13	0.40	312	NE	69	8.23	104	S	26	18.81	**fol**
11AS25	16	10	5	0.28	26	10	15	-0.19	9	5	4	0.01	184	W	61	8.93	19	E	32	14.57	**fol**
11AS28	15	10	5	0.33	22	14	7	0.35	16	2	13	-0.69	225	NW	72	6.07	107	S	33	15.93	**fol**
11AS38	9	7	2	0.49	17	9	8	0.06	20	18	2	0.80	18	SW	86	14.33	137	SW	14	15.99	**fol=lin**
11AS39	17	13	4	0.50	28	11	15	-0.12	26	16	9	0.27	228	NW	86	10.72	61	SE	3	11.59	**fol=lin**
11AS40b	15	12	2	0.65	16	13	3	0.65	20	16	3	0.64	204	NW	53	8.46	74	S	51	22.09	**fol**
11AS46b	9	5	4	0.16	11	8	4	0.35	11	8	3	0.38	128	SW	46	12.13	293	NE	47	27.33	**fol**
11AS47	14	9	4	0.43	18	10	8	0.10	29	14	13	0.06	232	NW	71	6.09	15	E	23	4.30	**fol=lin**
11AS52	18	13	4	0.50	45	31	11	0.45	90	47	30	0.19	244	NW	77	7.60	20	E	17	11.28	**fol**
11AS53	17	8	8	0.03	18	9	9	0.00	29	3	25	−0.75	212	NW	59	6.81	47	SE	32	10.46	**fol=lin**
11AS58	20	12	8	0.19	15	7	7	0.02	29	10	17	−0.25	267	N	57	27.67	73	SE	32	8.09	**lin**

Table 4. Mean susceptibility K_m, total magnetite content and number of magnetite grains in each sample.

Sample	K_m	K_m core	vol mgt	# mgt grains	vol% mgt
	10^{-3} SI	10^{-3} SI	mm^3		
11AS11	31	33	24.94228	3627	0.231
11AS12	27	22	26.31648	3532	0.244
11AS25	40	40	40.02171	11974	0.371
11AS28	44	45	28.61001	9268	0.265
11AS38	30	29	21.86912	3705	0.203
11AS39	34	37	41.87803	6137	0.388
11AS40	52	53	51.1365	6358	0.474
11AS46	108	119	155.4828	21715	1.440
11AS47	23	26	27.54967	2582	0.255
11AS52	36	38	25.60465	6658	0.237
11AS53	9	18	17.34516	2712	0.161
11AS58	33	28	32.31077	1931	0.299

vol core = 10799.2247 mm^3.